Journal of Applied Mathematics and Physics, 2024, 12, 2032-2040
https://www.scirp.org/journal/jamp
ISSN Online: 2327-4379
ISSN Print: 2327-4352

Effects of Crosswise Appendage Plate Flexibility on the Drag Reduction Characteristics of Cylinder

Jiyao Yang[1], Xiaomei Ye[2], Guoyi He[1], Feng Yu[1]

[1]The School of Aircraft Engineering, Nanchang Hangkong University, Nanchang, China
[2]The School of Foreign Languages, Nanchang Hangkong University, Nanchang, China
Email: jiyaoyang1019@163.com

How to cite this paper: Yang, J.Y., Ye, X.M., He, G.Y. and Yu, F. (2024) Effects of Crosswise Appendage Plate Flexibility on the Drag Reduction Characteristics of Cylinder. *Journal of Applied Mathematics and Physics*, **12**, 2032-2040.
https://doi.org/10.4236/jamp.2024.126124

Received: May 7, 2024
Accepted: June 10, 2024
Published: June 13, 2024

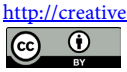

Abstract

In engineering applications (Like an ocean riser), fluid flow around bluff bodies generates substantial resistance, which can jeopardize structural integrity, lifespan, and escalate resource consumption. Therefore, employing drag reduction measures becomes particularly crucial. This paper employs the immersed boundary method to investigate the impact of transversely oriented appendage plate flexibility on the drag of cylinders under different Reynolds numbers and distances. The results indicate that flexible appendage plate exerts drag reduction effects on the downstream cylinder, with this effect gradually diminishing as Reynolds numbers increase. At identical Reynolds numbers, the drag reduction effect initially increases and then decreases with distance, with the optimal drag reduction distance observed at D = 2.5. Compared to cylinders without appendage plate, the maximum drag reduction achieved is 30.551%. Addressing the drag reduction issue in cylinders holds significant importance for ensuring engineering structural integrity, enhancing engineering efficiency, and developing novel underwater towing systems.

Keywords

Appendage Plate, Flexibility, Cylinder Flow, Drag Reduction

1. Introduction

Ocean risers are crucial components of offshore oil and gas production systems, serving as conduits for transporting hydrocarbons from the seabed to the surface facilities. Bluff body flow phenomena are commonly encountered in Ocean risers. When fluid flows around a bluff body, it generates significant resistance, which can compromise the structural integrity and service life of the system.

Additionally, overcoming this resistance consumes more energy. Therefore, employing methods to mitigate drag becomes particularly important. Over the years, researchers have conducted extensive studies on drag reduction for bluff body flow disturbances, with cylinder flow, as a typical representation of bluff body flow. There are also some similarities between the cylinder and the Marine riser in structure, being widely utilized in drag reduction research [1] [2] [3] [4].

Achenbach [5] delved into the study of flow-induced drag, unveiling that the primary resistance encountered by subsonic flow-disturbing bodies is pressure drag, which constitutes over 95% of the total drag. Consequently, reducing the pressure differential around the cylinder can effectively lower the cylinder's drag. Following this line of thought, the most direct approach involves introducing a passage between the fore and aft stagnation points of the cylinder to diminish the pressure differential. Izutsu [6] devised a slender slit along the axis of a solid cylinder, whereas Yajima and Sano [7] incorporated two rows of small holes along the axis of a hollow cylinder to alter surface pressures and delay airflow separation. Furthermore, Lesage and Gartshore [8] observed in their research that the drag on bodies (e.g., small cylinders, flat plates) positioned in the wake of disturbances can be significantly reduced. Alejandro and colleagues [9] explored the impact of appendages with different shapes (square, circular, rectangular, and elliptical) on the forces acting on cylinders and square prisms. The results reveal that the effect of appendages of diverse shapes on the drag experienced by the main cylinder and main square prism is dependent on their placement angles. Overall, among the four shapes of appendages, elliptical ones exhibit the most effective drag reduction, followed by rectangular, circular, and square shapes.

Prasad and Williamson [10] studied the effects of longitudinally oriented appendage plate placed upstream of a cylinder on its drag forces. Through modifications in appendage size and positioning, they identified that the most pronounced drag reduction occurred when the plate was situated 3/2D width away from the cylinder and had dimensions of 1/3D (with D denoting the cylinder diameter).

This study utilizes the immersed boundary technique to conduct numerical simulations of the drag effects induced by rigid and flexible transverse appendage plate (Kb = 0.01) ahead of the cylinder, considering different Reynolds numbers (Re = 150/200/255) and distances (D = 2.0/2.5/3.0/3.5). The aim of this paper is to provide reference for reducing the drag caused by blunt body turbulence in Marine risers by studying the influence of the flexibility of the appendage plate on the resistance characteristics of the cylinder. Researching drag reduction in cylinders is of paramount importance for safeguarding engineering structures, resource conservation, improving engineering efficiency, and innovating new underwater towing systems [11].

2. Physical Model and Numerically Method

2.1. Physical Model

In this paper, the numerical simulation is carried out by the immersed boundary

method. The experimental device is shown in Figure 1. The rigid/flexible appendage plate, affixed at the leading edge, is centrally located in front of the cylinder. With the exception of the leading edge point, all other points on the flexible appendage plate are capable of independent movement in the x and y directions (the rigid appendage plate remains static in the x and y directions). Both are situated within a two-dimensional, uniform, incompressible inflow from left to right. In the figure, U_∞ represents the inflow velocity; D represents the horizontal distance from the cylinder's front end to the tip of the appendage plate; L represents the length of the appendage plate. The calculation regions in this article are: $-5l < x < 20l$ and $-8l < y < 8l$. The middle encryption area is $-l < x < 6l$ and $-2l < y < 2l$, and the grid spacing is $\Delta h/l = 0.02$.

2.2. Numerically Method

The core idea of the immersion boundary method is to model the complex structure boundary of the immersed object into a force in the Navier-Stokes momentum equation, so as to replace the effect of the object boundary on the flow field.

The governing equation is:

$$\frac{\partial u}{\partial t} = \nabla \cdot (uu) = -\nabla p + \frac{1}{Re}\nabla^2 u + f \tag{1}$$

$$\nabla \cdot u = 0 \tag{2}$$

$$f(x,t) = \int_0^{L_b} F(X(s),t)\delta(x - X(s))\mathrm{d}s \tag{3}$$

$$U(X(s),t) = \int_\Omega u(x,t)\delta(x - X(s))\mathrm{d}x \tag{4}$$

In the above formula, $u(x,t)$ is the fluid velocity, $p(x,t)$ is the fluid pressure, Re is the dimensionless Reynolds number, $Re = \rho d U_\infty / \mu$, F is the introduced external force, representing the force on the fluid caused by the immersed object boundary, X is the coordinate of the appendage plate, the force between the immersed boundary and the flow field is calculated by the immersion boundary method, and the update of the appendage plate position is as follows:

$$\frac{\partial X}{\partial t} = U(X(s),t) \tag{5}$$

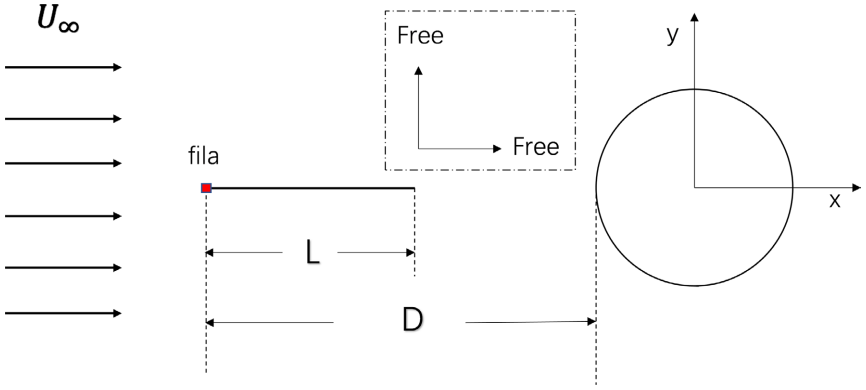

Figure 1. Schematic contour of calculation model.

where, $X(s)$ is the position coordinate of the appendage plate, and s represents the Lagrangian coordinate of the appendage plate, whose boundary conditions are defined as follows: Free boundary condition of the appendage head ($s = 0$): $X(s=0,t=0)=(x_0,0)$, $\partial^2 X/\partial s^2=(0,0)^{\mathrm{T}}$, free boundary condition of the tail of the appendage plate ($s = L$): $T=0, \partial^2 X/\partial s^2=(0,0)^{\mathrm{T}}$.

The interaction between the immersion boundary and the fluid consists of two components:

$$F(s,t)=F_1(s,t)+F_2(s,t) \tag{6}$$

$F(s,t)$ is the interaction force between the fluid and the immersed boundary, where $F_1(s,t)$ is the interaction force between the fluid and the solid cylinder, and $F_2(s,t)$ is the interaction force between the fluid and the flexible appendage plate. The equation $F_2(s,t)$ for the interaction between the fluid and the flexible appendage plate is calculated as follows:

$$F_2(s,t)=F_s(s,t)+F_b(s,t)=\frac{\partial T\hat{\boldsymbol{\tau}}}{\partial s}+\frac{\partial E_b}{\partial X} \tag{7}$$

$$T=K_s\left(\left|\frac{\partial \boldsymbol{X}}{\partial s}\right|-1\right) \tag{8}$$

$$\hat{\boldsymbol{\tau}}=\frac{\dfrac{\partial \boldsymbol{X}}{\partial s}}{\left|\dfrac{\partial \boldsymbol{X}}{\partial s}\right|} \tag{9}$$

$$E_b=\frac{1}{2}K_b\int\left|\frac{\partial^2 \boldsymbol{X}(s,t)}{\partial s^2}\right|^2 \mathrm{d}s \tag{10}$$

$F_s(s,t)$ is the tensile force and compression force of the appendage plate; $F_b(s,t)$ is the bending force; T is the tension of the appendage plate, which is obtained from Hooke's law. For details, see Formula (8). $\hat{\boldsymbol{\tau}}$ is defined on the appendage plate each point unit tangent vector, as shown in formula (9). E_b is the bending energy of the appendage plate, see Equation (10). K_s is the tensile coefficient of the appendage plate ($K_s = 1 \times 10^2$). K_b is the bending stiffness of the appendage plate.

In Lin's study [12], by simulating the oscillation of a cylinder in a uniform flow and the motion of appendage plate in a cylindrical turbulent flow, the solution program used in this paper is verified to be correct.

3. Calculation Results and Analysis

As depicted in **Table 1**, the experimental design involves selecting a rigid/flexible appendage plate of length L = 1.0 and placing it horizontally in front of the cylinder. A total of twenty-four numerical simulation experiments are conducted under different Reynolds numbers (Re = 150/200/255) and distances (D = 2.0/2.5/3.0/3.5). The resulting drag coefficients of the cylinder with rigid/flexible appendage plates are then contrasted with those of a solitary cylinder in the flow

field, facilitating an analysis of the influence of rigid/flexible appendage plates on cylinder drag reduction efficiency.

3.1. The Influence of Appendage Plate on the Drag Coefficient of the Cylinder

For $D = 2.0$, the graph in Figure 2 illustrates the changes in the cylinder's drag coefficient under various conditions. The legend indicates that $Re = 150$ represents the drag coefficient variation of the cylinder at Reynolds number 150, $Re = 150\text{-}R$ represents the drag coefficient variation of the cylinder with a rigid appendage plate, and $Re = 150\text{-}F$ represents the drag coefficient variation of the

Table 1. Experimental scheme.

Experimental object	D	Reynolds number	L
Rigid attachment plate	2.0	150/200/255	1.0
	2.5	150/200/255	1.0
	3.0	150/200/255	1.0
	3.5	150/200/255	1.0
Flexible attachment plate	2.0	150/200/255	1.0
	2.5	150/200/255	1.0
	3.0	150/200/255	1.0
	3.5	150/200/255	1.0
Cylinder	---	150/200/255	---

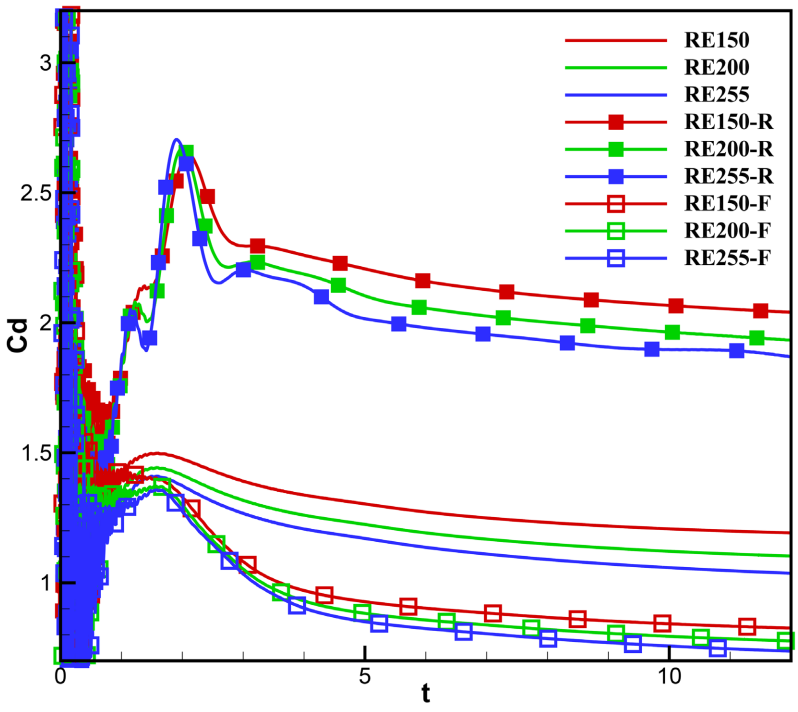

Figure 2. Variation of cylindrical drag coefficient at different Reynolds numbers $D = 2.0$.

cylinder with a flexible appendage plate.

Within Figure 2, the nine distinct sets of simulation results are segmented into three discernible sections. It is evident that the addition of rigid appendage plates to the cylinder significantly increases its drag coefficient compared to the cylinder in the flow field, whereas the cylinder positioned behind the flexible appendage plates exhibits a notably lower drag coefficient than the cylinder in the flow field. Similarly, the drag coefficients of the cylinders under different conditions decrease with increasing Reynolds numbers. Subsequently, a quantitative analysis will be conducted.

In Figure 2, the drag coefficients of the cylinders under different conditions exhibit considerable fluctuations within the first 5 seconds, gradually stabilizing between 5 and 12 seconds. For subsequent quantitative analyses, the average drag coefficients from the 5 to 12-second period are selected. As indicated in Figure 2, when D = 2.0, the addition of rigid appendage plates results in a 70.58% increase in the drag coefficient (from 1.234 to 2.105), a 74.09% increase (from 1.150 to 2.002), and a 77.156% increase (from 1.090 to 1.931) at Reynolds numbers of 150, 200, and 255, respectively, compared to a cylinder in a standalone flow field. Under the same conditions, adding flexible appendage plates reduces the drag coefficient by 29.74% (from 1.234 to 0.867), 28.70% (from 1.150 to 0.820), and 28.07% (from 1.090 to 0.784).

In Figure 3, the changes in the drag coefficient of the cylinder at various positions behind rigid/flexible appendage plates are depicted. During the stable phase (5 - 12 s), the drag coefficient of the cylinder decreases progressively with distance behind rigid appendage plates, whereas the drag reduction effect of flexible appendage plates shows an initial increase followed by a decrease as distance increases. The optimal drag reduction distance in the experiment is D = 2.5.

Further analysis, the reduction in the mitigating effect of distance on drag

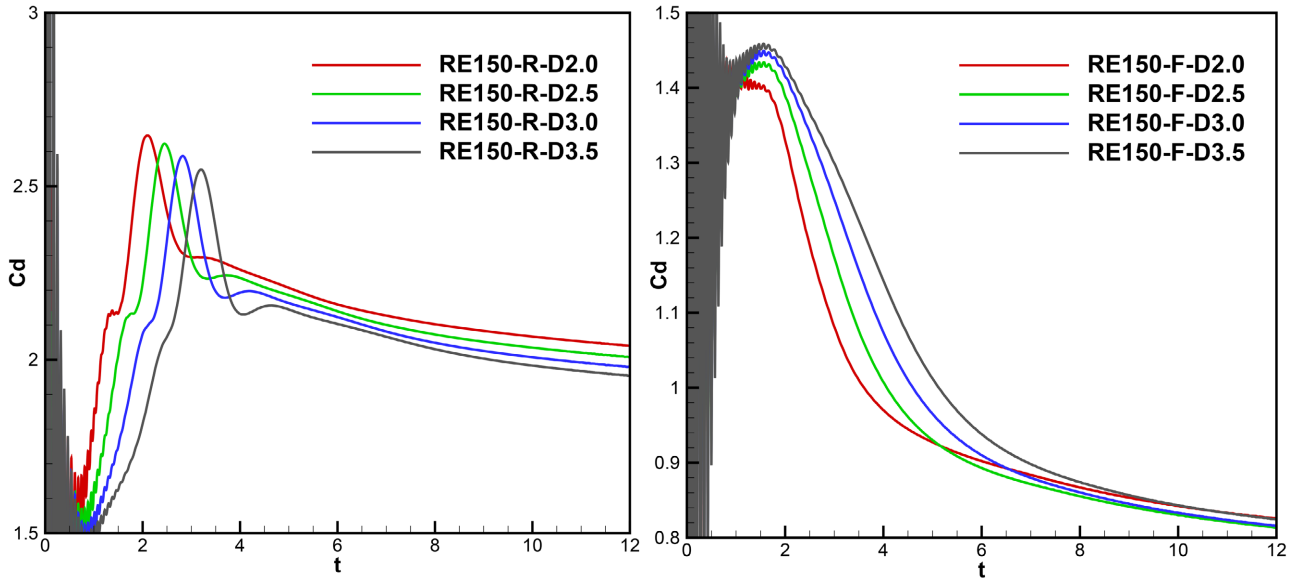

Figure 3. Resistance coefficient with distance (left rigid, right flexible).

increase by rigid plates diminishes with increasing Reynolds numbers. When compared to conditions with D = 2.0, at Re = 150/200/255, it exhibits drag reduction percentages of 3.515%, 2.547%, and 1.812%, respectively, for D = 3.5. As the Reynolds number increases, the distance behind the flexible appendage plates has no notable effect on the drag reduction of the cylinder, all remaining around 3% (Compared to D = 2.5 conditions, at Re = 150/200/255, the drag increases by 3.267%, 3.210%, and 3.493%, respectively, for D = 3.5).

3.2. Analysis of the Influence of Appendage Plate on the Drag Coefficient of the Cylinder

To explore the mechanism of appendages on the drag coefficient of the cylinder, the upstream fluid flow velocity was monitored, the result shows that placement of rigid appendages increases the horizontal velocity of the upstream fluid flow, resulting in a larger impact force on the cylinder's leading edge and an increase in static pressure at the stagnation point, as shown in Figure 4. When the flow encounters flexible appendages, they induce slight oscillations, deflecting the flow and creating a vortex-free region resembling a triangle upstream of the cylinder. Compared to the scenario without flexible appendages, this reduces the horizontal flow velocity by nearly 9 times, leading to a decrease in the impact force on the cylinder's leading edge and a reduction in static pressure at the stagnation point, as depicted in Figure 4. Pressure contour plots around the cylinder under three different conditions are shown in Figure 5. Behind flexible appendages, the static pressure at the stagnation point is around 0.4, whereas it is approximately 1.2 without appendages and roughly 2 behind rigid appendages. The reason why the flexible appendage plate can reduce the resistance of the cylinder is that under the action of incoming flow, the appendage plate located in front of the cylinder generates vibration and plays a role in guiding the flow, which reduces the incoming flow speed directly in front of the cylinder, decreases the stagnation point pressure, decreases the pressure difference between the front and back of the cylinder, and decreases the pressure difference resistance, resulting in the reduction of the cylinder resistance coefficient.

4. Conclusions

This study, employing the immersed boundary method, investigated the influence

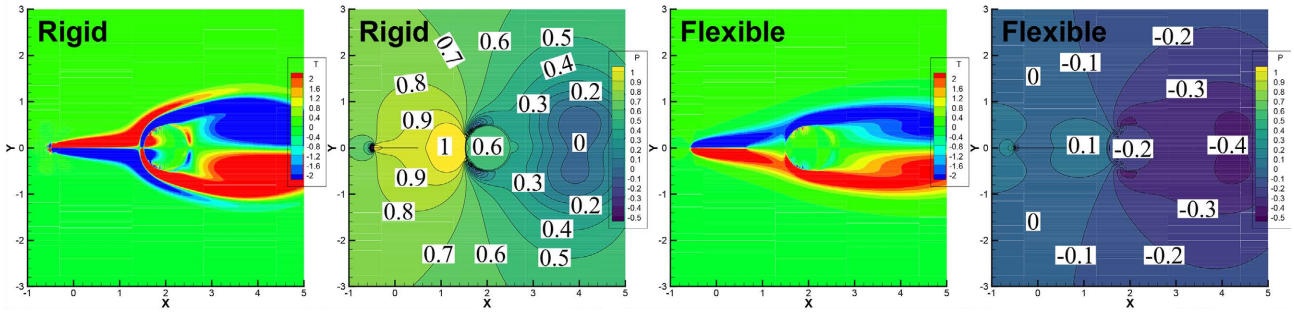

Figure 4. Vorticity and pressure diagrams of flexible/rigid appendages.

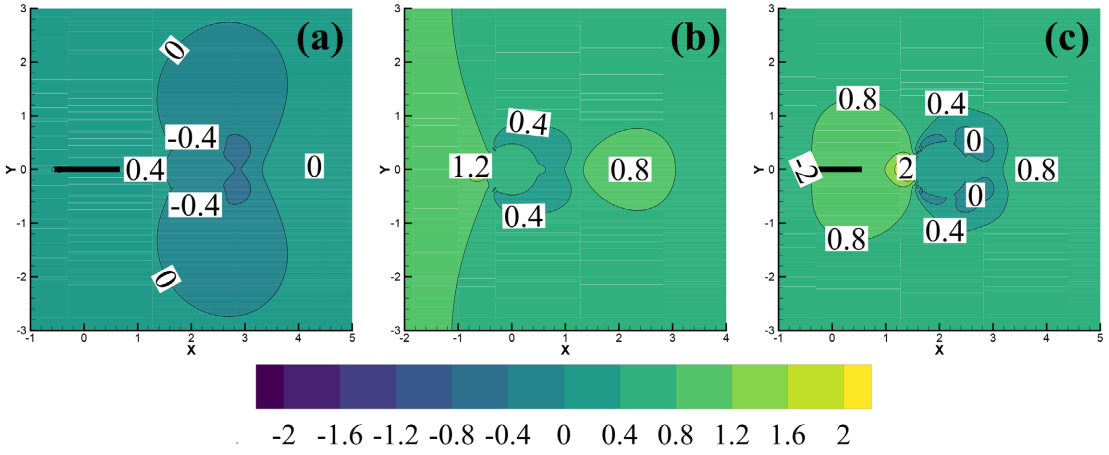

Figure 5. Pressure contour comparison diagram: (a) Cylinder behind Flexible Appendages, (b) Cylinder, (c) Cylinder behind Rigid Appendages.

of transversely oriented appendage plate flexibility on the drag of cylinders under different Reynolds numbers and distances. The following conclusions were drawn:

1) Rigid appendage plate induces drag augmentation on cylinders, with the augmentation effect increasing as Reynolds numbers rise. At identical Reynolds numbers, the augmentation effect gradually diminishes with increasing distance.

2) Flexible appendage plate contributes to drag reduction on cylinders, with the reduction effect decreasing as Reynolds numbers increase. At identical Reynolds numbers, the drag reduction effect initially increases and then decreases with increasing distance. The optimal drag reduction distance observed in the experiments is $D = 2.5$.

Acknowledgements

This work is supported by the National Natural Science Foundation of China (grant number 12362026 and 11862017).

Conflicts of Interest

The authors declare no conflicts of interest regarding the publication of this paper.

References

[1] Ji, W.Y. (2008) Three-Dimensional Numerical Simulation Study on the Drag Reduction Characteristics of Cylinder Flow around Appendages. Harbin Institute of Technology, Harbin. (In Chinese)

[2] Su, L.G., Gu, J.J., Duan, M.L., *et al.* (2015) Analysis of Flow Field Characteristics around Cylinder Based on CFD. *Oil Field Equipment*, **44**, No. 4. (In Chinese)

[3] Song, Z.H. and Duan, M.L. (2016) Study on the Suppression Effect of Three Appendages on Vortex Shedding of Marine Risers. *Petroleum Machinery*, **44**, No. 6. (In Chinese)

[4] Liu, F.X. (2019) Numerical Simulation Study on the Influence of Appendages on

Cylinder Vibration and Wind Energy Harvesting Characteristics. Harbin Institute of Technology, Harbin. (In Chinese)

[5] Achenbach, E. (1968) Distribution of Local Pressure and Skin Friction around a Circular Cylinder in Cross-Flow up to Re = 5×10^6. *Journal of Fluid Mechanics*, **34**, 625-639. https://doi.org/10.1017/S0022112068002120

[6] Izutsu, N. (1993) Fluid Force Measurements for a Circular Cylinder with a Slit. *Nagare*, **12**, 293-301.

[7] Yajima, Y. and Sano, O. (1996) A Note on the Drag Reduction of a Circular Cylinder due to Double Rows of Hole. *Fluid Dynamics Research*, **18**, 237-243. https://doi.org/10.1016/0169-5983(96)00015-9

[8] Lesage, F. and Gartshore, I.S. (1987) A method of Reducing Drag and Fluctuating Side Force on Bluff Bodied. *Journal of Wind Engineering and Industry Aerodynamics*, **25**, 229-245. https://doi.org/10.1016/0167-6105(87)90019-5

[9] Alonzo-García, A., *et al.* (2021) The Control of Unsteady Forces and Wake Generated in Circular and Square Cylinder at Laminar Periodic Regime by Using Different Rod Geometries. *Ocean Engineering*, **233**, Article ID: 109121. https://doi.org/10.1016/j.oceaneng.2021.109121

[10] Prasad, A. and Williamson, C.H.K. (1997) A Method for the Reduction of Bluff Body Drag. *Journal of Wind Engineering and Industrial Aerodynamics*, **69-71**, 155-167. https://doi.org/10.1016/S0167-6105(97)00151-7

[11] Jiang, X.L., Ouyang, L.H. and Li, C. (2022) Research on Drag Reduction Performance of Cylinder Based on Surface V-Shaped Grooves. *Digital Ocean and Underwater Defense*, **5**, No. 2. (In Chinese)

[12] Lin, X., He, G., He, X., Wang, Q. and Chen, L. (2017) Numerical Study of the Hydrodynamic Performance of Two Wiggling Hydrofoils in Diagonal Arrangement. *Journal of Applied Mathematics and Physics*, **3**, 31-38. https://doi.org/10.4236/jamp.2017.51005